Available online at www.sciencedirect.com
ScienceDirect
Remote Sensing of Environment 112 (2008) 391–402
Remote Sensing of Environment
www.elsevier.com/locate/rse

Mapping surface roughness and soil moisture using multi-angle radar imagery without ancillary data

M.M. Rahman [a,*], M.S. Moran [a], D.P. Thoma [a], R. Bryant [a], C.D. Holifield Collins [a], T. Jackson [b], B.J. Orr [c], M. Tischler [d]

[a] USDA ARS Southwest Watershed Research Center, Tucson, Arizona, USA
[b] USDA-ARS Hydrology and Remote Sensing Laboratory, Washington DC, USA
[c] Office of Arid Land Studies, University of Arizona, Tucson, Arizona, USA
[d] US Army Engineer Research and Development Center, Topographic Engineering Center, Alexandria, Virginia, USA

Received 4 April 2006; received in revised form 26 September 2006; accepted 31 October 2006

Abstract

The Integral Equation Model (IEM) is the most widely-used, physically based radar backscatter model for sparsely vegetated landscapes. In general, IEM quantifies the magnitude of backscattering as a function of moisture content and surface roughness, which are unknown, and the known radar configurations. Estimating surface roughness or soil moisture by solving the IEM with two unknowns is a classic example of under-determination and is at the core of the problems associated with the use of radar imagery coupled with IEM-like models. This study offers a solution strategy to this problem by the use of multi-angle radar images, and thus provides estimates of roughness and soil moisture without the use of ancillary field data. Results showed that radar images can provide estimates of surface soil moisture at the watershed scale with good accuracy. Results at the field scale were less accurate, likely due to the influence of image speckle. Results also showed that subsurface roughness caused by rock fragments in the study sites caused error in conventional applications of IEM based on field measurements, but was minimized by using the multi-angle approach.

Keywords: Soil moisture; Surface roughness; Radar; ENVISAT-ASAR; Integral Equation Model; Active microwave

1. Introduction

Information about the distribution of surface soil moisture (θ_S) is important for a number of applications ranging from the management of agriculture and natural resources to the science of understanding land–atmosphere interaction to determining vehicle mobility. Images of radar backscatter from orbiting sensors have been used for mapping surface soil moisture (Moran et al., 2004). Retrieval of θ_S from radar backscatter (σ^0) is often based on radar backscatter models, such as the Integral Equation Model (IEM), which was developed for bare soil, but can be used with sparse vegetation (Fung, 1994; Fung & Pan, 1986; Fung et al., 1992). In general terms, IEM represents the radar backscatter of an image with known radar configurations as a function (f) of θ_S and surface roughness, where

$$\sigma^0 = f(h_{RMS}, L_c\theta_S). \quad (1)$$

The model characterizes surface roughness by the root mean squared height (h_{RMS}) variation of the surface at centimeter scale and the correlation length (L_c) of the same height variation. It is conventionally measured by a pin meter, and more recently, by field-deployed laser scanners (both described by Bryant et al. (2007)).

Recent studies have indicated that the magnitude of h_{RMS} and L_c are scale related (Le Toan et al., 1999) and highly dependent on the length of the transect (Bryant et al., 2007), when measured with a pin meter or laser scanner. This is true especially for the estimate of L_c (Bryant et al., 2007; Davidson et al., 2000). The suggestions for optimum transect length vary

* Corresponding author.
E-mail address: magfur@sasktel.net (M.M. Rahman).

0034-4257/$ - see front matter © 2007 Published by Elsevier Inc.
doi:10.1016/j.rse.2006.10.026

from a couple of meters (Baghdadi et al., 2000) to hundreds of meters (Verhoest et al., 2000). L_c also depends on the type of auto correlation function used in its estimation from field data (Baghdadi et al., 2004; Davidson et al., 2000). This implies that consistent roughness parameters may not be estimated using field data for use as an input to the IEM. Moreover, conducting field measurement of roughness may become impractical and expensive when large areas need to be covered.

In addition to the field measured roughness, the abundance of rock fragments, if present in study locations, may influence radar-perceived roughness. The radar signal penetrates a few centimeters below the ground and is likely to be affected by the subsurface nature of roughness caused by rock fragments below the soil surface (Jackson et al., 1992). When the radar signal penetrates a few centimeters below the ground surface, it experiences multiple bounce by the subsurface rock fragments, which may result in volume scattering. It is likely that the radar-perceived roughness is a combination of surface and subsurface roughness. On the other hand, the pin meter measures roughness at the top of the soil surface and is not designed to measure the roughness caused by the subsurface rock fragments.

For all these reasons, measurement of distributed surface roughness has been a barrier for regional application and wide use of microwave technology for surface soil moisture sensing. It would be beneficial to develop a surface roughness mapping system based solely on satellite data and a radar backscatter model, eliminating the need for field measurements altogether. In such a situation, an operational soil moisture assessment system based on a radar backscatter model would be practical. Furthermore, maps of surface roughness may have potential usefulness based on their own merit. The availability of image-based roughness maps may provoke future applications to erosion prediction, surface runoff modeling and soil moisture estimation from passive microwave imagery.

Many components of research needed to develop an image-based approach have already been published and can be compiled to develop a method for mapping of roughness and soil moisture. Zribi and Dechambre (2002) indicated an interesting property of IEM that may have great use. They found that the difference in backscatter ($\Delta\sigma^0$) generated by the IEM model with two different incidence angles, keeping all other parameters constant, is in proportion to roughness only. It was found that $\Delta\sigma^0$ is proportional to the ratio of h_{RMS} and L_c, which was referred to as the z-index and defined as h_{RMS}^2/L_c. Z-index is computed by Zribi and Dechambre (2002), where

$$h_{RMS}^2/L_c = g(\Delta\sigma^0). \tag{2}$$

This equation is generally valid when the difference in incidence angles is large and surface moisture conditions remain unchanged. Here, 'g' is a function, the specific form of which can be estimated using IEM simulated data. This formulation provides a foundation for mapping of surface roughness using radar imagery with two incidence angles. However, the formulation does not provide an explicit solution of h_{RMS} and L_c, which are needed as inputs to IEM for the retrieval of surface soil moisture from radar imagery.

As a complement to the work by Zribi et al., Rahman et al. (2007) expressed the relation between h_{RMS} and L_c using simple equations based on IEM theory. Then, using a radar image obtained with relatively dry surface condition (θ_S on the order of 0.03 m^3 m^{-3}), they showed that it was possible to derive both h_{RMS} and L_c from the measurement of radar backscatter. That is, the effect of θ_S on the σ^0 of a radar signal measured in the dry season (σ^0_{dry}) is very low and this was neglected altogether without making significant error. IEM simulation indicates that 0.03 m^3 m^{-3} deviations in the soil moisture may cause error up to 1 db (Rahman et al., 2007), when the moisture condition is low. Considering the stated absolute accuracy of the radar sensor is approximately 1 dB (Staples & Branson, 1998), this error may be acceptable. The general form of the equation was written as

$$\sigma^0_{dry} = h(h_{RMS}L_c). \tag{3}$$

This equation holds over certain incidence angle ranges, usually 30 to 50°. The specific form of the equation was estimated using IEM simulated data for certain radar configurations (Rahman et al., 2007).

Substituting terms between Eqs. (2) and (3) it should be possible to solve for two roughness parameters, h_{RMS} and L_c, explicitly, where

$$\left.\begin{aligned} L_c &= \omega(\Delta\sigma^0, \sigma^0_{dry}), \text{ and} \\ h_{RMS} &= \psi(\Delta\sigma^0, \sigma^0_{dry}). \end{aligned}\right\} \tag{4}$$

Here, ω and ψ are two functions determined by substitution of terms. The resulting roughness maps then can be used to parameterize IEM for producing surface soil moisture map.

As evident in this formulation, a maximum of three radar images are needed for roughness mapping. These include two images with different incidence angles to determine $\Delta\sigma^0$ and one image with dry ground condition to measure σ^0_{dry}. The image requirements can be reduced to two if the images at two incidence angles are available for dry surface conditions. In this case, one of them can be used for extracting σ^0_{dry} and both can be used to extract $\Delta\sigma^0$. The images required for computing $\Delta\sigma^0$ can be acquired with either dry or wet surface conditions. However, the moisture content of the ground surface has to remain unchanged during acquisition of these two images, since $\Delta\sigma^0$ is modeled as a function of roughness only (Eq. (2)). Moreover, the roughness itself has to remain unchanged during acquisition of all images, since the goal is to solve for the roughness parameters from images.

In spite of these limitations, data from currently orbiting radar sensors can be used to resolve Eq. (4) and determine both h_{RMS} and L_c for IEM parameterization. In the second step, the values of h_{RMS} and L_c can be substituted in Eq. (1) and expressed as

$$\sigma^0_{wet} = \lambda(\Delta\sigma^0, \sigma^0_{dry}, \theta_S), \tag{5}$$

where the subscript "wet" in σ^0_{wet} is used to distinguish it from backscatter of a dry surface (σ^0_{dry}), as defined earlier. Eq. (5) then can be inverted for solving surface soil moisture, where

$$\theta_S = \lambda^{-1}(\Delta\sigma^0, \sigma^0_{dry}, \sigma^0_{wet}). \quad (6)$$

Here, $\Delta\sigma^0$ and σ^0_{dry} are functions of roughness parameters, such as $\Delta\sigma^0(h_{RMS}, L_c)$ and $\sigma^0_{dry}(h_{RMS}, L_c)$, which in turn implies that θ_S is modeled in Eq. (6) as function of roughness and σ^0_{wet}. In the presence of integrals and Fourier transform in the 'λ' function of IEM, it is difficult, though not impossible, to get an inverse. This difficulty can be overcome by an approximation of Eq. (6) with a polynomial of required order. IEM simulated data can be used for this purpose.

Since the solution of all parameters, such as h_{RMS}, L_c and θ_S, can be obtained through simultaneous use of images as described above, pixel-by-pixel computation can be implemented to derive the outputs in the form of maps.

The specific objectives of this study are as follows:

1) Implement the method outlined above for mapping characteristic parameters of surface roughness by the use of two Envisat ASAR images (June 9 and June 15, 2004) obtained under dry surface conditions;
2) Compare image-based measurements of h_{RMS} and L_c with conventional pin meter measurements for 13 sites in the semiarid Walnut Gulch Experimental Watershed (WGEW) near Tucson, Arizona;
3) Use the resulting roughness map to parameterize IEM for mapping soil moisture from two more Envisat ASAR images (July 14 and August 2, 2004) of WGEW under relatively wet ground condition; and
4) Validate the resultant surface soil moisture maps with field measurements of the same 13 sites during the overpass of Envisat on July 14 and August 2, 2004.

2. Materials and methods

To achieve research objectives, a study was conducted in Arizona in 2004, where a range of radar remote sensing data, and field collected roughness and soil moisture data was used. The IEM model approximated by simple functions were applied to the radar data for estimation of soil moisture and surface roughness, which were then compared with the field collected data.

2.1. Study site

This field study was conducted in the 150 km^2 Walnut Gulch Experimental Watershed (WGEW) operated by United States Department of Agriculture, Agriculture Research Service (USDA-ARS). The watershed is located in the Sonoran desert, State of Arizona, near the US–Mexico border. The watershed has a semi-arid climate in which the average annual rainfall is 330 mm. It is characterized by rolling hills ranging in elevation from 1220 to 1960 m and the major soil type is sandy loam with rock fragment fractions on the order of 47% by volume within the top few centimeters of the soil surface (USDA–NRCS, 2002). The watershed has sparse vegetation, consisting mainly of desert grass and shrub. There are many ephemeral streams and channels running across the watershed with no perennial water supply or source. The watershed is instrumented with precipitation gages, meteorological stations, soil moisture sensors and flumes for hydrologic experimentations (Renard et al., 1993).

2.2. Satellite data processing

Four Envisat ASAR images were used in this study; the specific type of the product is Alternating Polarization Ellipsoid Geocoded, which is described in the ASAR product handbook (ESA, 2002). Some of the features of the images used for analysis in this study are given in Table 1.

The image digital numbers (DN) are in units of amplitude and were converted to backscatter values (σ^0) following the ASAR product handbook. The computation of σ^0 was

$$\sigma^0 = \frac{\langle A^2 \rangle}{K} \sin\alpha, \quad (7)$$

where σ^0 is the radar backscatter in power [m^2/m^2], A is the pixel intensity in amplitude values, K is the external calibration constant [m^2/m^2] and α is the distributed incidence angle. The external calibration constant and distributed incidence angles of a particular image are found by performing header analysis using 'BEST' software (www.envisat.esa.int). The backscatter is converted from power to decibel unit (dB) for the use in the

Table 1
Sensor configuration of radar imagery used in this study

Envisat ASAR				
Image data	June 9, 2004	June15, 2004	July 14, 2004	August 2, 2004
Purpose	Roughness mapping	Roughness mapping	Soil moisture mapping	Soil moisture mapping
Pixel resolution	12.5 m	12.5 m	12.5 m	12.5 m
Used polarization	VV	VV	VV	VV
Image swath	IS6	IS2	IS6	IS5
Incidence angle	41.08°	24.8°	41.08°	37.39°
Frequency	C-band (5.3 GHz)	C-band (5.3 GHz)	C-band (5.3 GHz)	C-band (5.3 GHz)
Wavelength	5.6 cm	5.6 cm	5.6 cm	5.6 cm
Time of overpass	10:16 am	10:27 am	10:16 am	10:19 am

analysis. Power to decibel conversion is a logarithmic conversion, where

$$\sigma^0(\mathrm{dB}) = 10[\log\ (\sigma^0)]. \quad (8)$$

The ASAR images acquired on June 9 and June 15, 2004 were coincident with dry surface conditions and were used for the roughness mapping. The two images were selected so that the difference in incidence angles was the largest possible. IEM simulations suggest that the backscatter differences become more sensitive to surface roughness as the difference in incidence angle increases and are helpful for estimation of roughness. The ASAR images acquired on July 14 and August 2, 2004 corresponded to relatively wet surface conditions and were used for soil moisture mapping.

A median filter consisting of a 9-pixel moving window was applied for optimal speckle reduction (Thoma et al., 2006). Despite the filtering, some extreme high and low values of radar backscatter were detected in all output maps. Particular pixel values that deviated from the mean value of pixels (plus or minus) by more than three times the standard deviation were considered extreme values. The prevalence of extreme values was not large, and they seemed to associate with the mountain tops and surrounding areas, indicating likely effects of topography on the radar backscatter. A mode filter based on a 3-pixel moving window was applied over the image to replace extreme values with the mode of the surround values. This filter was effective in relatively flat areas where extreme values were less prevalent. In mountainous regions, a second pass of another mode filter based on a 10-pixel moving window was needed.

A good image-to-image registration was essential for this study since backscatter of corresponding pixels of two images were differenced in computing roughness of that pixel. Visual inspection indicated that the geocoded images that were used in this study had good image-to-image registration; therefore, further image registration was not applied. However, deviations up to three pixels were observed in image-to-ground registration in some parts of the study area, when geocoded images were compared with geo-registered aerial photographs. The accuracy of the computation needed for mapping surface roughness should be unaffected by this deviation, however, the deviation may affect the validation process. For validation of the results, that is, comparing output maps values with field data, an area of 110 by 110 m corresponding to each sample site was extracted from the roughness and soil moisture maps based on their known coordinates and was clipped. The averages of the values within clipped areas were compared with the field measurements of roughness and soil moisture. The 3-pixel deviation in registration may have affected the clipping part of validation process. To check if the 3-pixel deviation in registration had an impact, the size of the clipped area was increased to 150 by 150 m and the validation process was repeated. The increase in window size used for clipping was likely to capture effects of 3-pixel registration error.

2.3. Ground measurements of soil moisture and roughness

The top 5-cm surface soil moisture (θ_S) was measured at 13 sites over the two most dominant soil types of the WGEW (very gravelly sandy loam Elgin–Stronghold complex and very gravelly sandy loam Luckyhills–McNeal complex) at the time of Envisat overpasses on July 14 and August 2, 2004. Depending on the level of moisture, approximately 20–30 measurements were made with a Theta Probe over a 110 by 110 m area at each of the 13 sites. The objective of these measurements was to capture the spatial variability of θ_S over 9×9 Envisat image pixels for each training site. The time span over which the field measurements were undertaken was divided equally before and after the satellite overpass. Soil moisture data during dry season overpass of Envisat (June 9 and June 15, 2004) was measured with a Vitel Probe installed at 5 cm depth at all 13 sites for automatic and year round monitoring of soil moisture. For the WGEW study site, the abundance of rock fragments may have caused problems for the Theta Probe or Vitel Probe to capture the true moisture content of the soil. The problem caused by the presence of rock fragments is the differential content of moisture in soil and in rock fragments of the targeted material. Rock fragments have little moisture even when the surrounding soil is saturated. Radar backscatter may be sensitive to moisture content of rock–soil composite as opposed to the moisture content of the soil only measured by the Theta Probe signal. The pins of the Theta Probe instruments need to penetrate into the soil in order to get a moisture reading. This requires a spot on the ground that has negligible amount of rock fragments. A rock fragment correction was made by subtracting the rock fraction effect from the field measure of volumetric soil moisture in the manner described by Thoma et al. (2006). The adjustment involves reducing the field measured moisture content by the average proportion of rock fragment in the study site, which is 47%, to represent moisture content of rock–soil composite. This computation was based on the assumption that the rock contains negligible amounts of moisture and the Theta Probe measured moisture constitutes the soil portion of the rock–soil composite. It was further assumed that all experiment locations have the same rock fragment content, the magnitude of which is equal to the watershed average. This later assumption may have some implication to the accuracy of the result, given the unavailability of rock fragment data for all study locations.

Field data collected from 13 sites spread over 150 km^2 of WGEW were summarized in Table 2. The moisture content of the study site was generally low, with an average of roughly 0.05 during the study period. The average moisture content was 0.04 $m^3\ m^{-3}$ in July and had increased to 0.07 $m^3\ m^{-3}$ in August. The variability of moisture content across space was greater (0.02 to 0.06 $m^3\ m^{-3}$ in July, and 0.02 to 0.10 $m^3\ m^{-3}$ in August). The soil moisture contents were the same in June 9 and June 15 (0.03 $m^3\ m^{-3}$).

Surface roughness for the 13 sample sites was measured using a pin meter of 3-m profile length in December, 2004. The pin meter traced the surface height variation at 1-cm intervals and the trace was documented in a photograph with a digital camera. Ten pin-meter measurements were made randomly over an area of 35×35 m around each sample site. The photographs were processed with a computer program to generate values of h_{RMS} and L_c averaged over each site (Bryant et al., 2007). An

Table 2
Summary statistics of field measured moisture content (θ_S), roughness RMS height (h_{RMS}) and correlation length (L_c)

Field measurements, 13 sites	June 9, 2004	June15, 2004	July 14, 2004	August 2, 2004
Moisture content[a] (θ_S), in m^3 m^{-3}				
Mean	0.03	0.03	0.04	0.07
SD	0.01	0.01	0.01	0.01
Surface roughness in cm				
Mean h_{RMS}	0.79			
SD h_{RMS}	0.29	Conducted once in December, 2004		
Mean L_c	8.20			
SD L_c	2.47			

[a] Correction for rock fragment applied.

exponential autocorrelation function was assumed for computing L_c. This assumption was based on an experiment in which exponential and Gaussian correlation functions were used for estimation of L_c and the exponential function worked better with these data. This method of measuring roughness may have some limitations. When radar signal penetrates a few centimeters below ground surface it experiences multiple bounce by the subsurface rock fragments, which results in volume scattering. This is in addition to the scattering due to surface roughness. As a result, radar-perceived roughness is likely larger than that of field measurements. The roughness measuring field device, the pin meter, is not designed to account for subsurface nature of roughness. Therefore, roughness measurements by the pin meter may not be adequate to characterize surface roughness for input to IEM, especially for study sites with large amounts of rock fragments.

The average h_{RMS} across all sites was found to be 0.79 cm, with a maximum of 1.3 cm and a minimum of 0.48 cm. The average field measurement for L_c was 8.2 cm, ranging from 5.0 cm to 12.2 cm.

2.4. Radar model and implementation

The Integral Equation Model (IEM) is the most widely-used, physically based radar backscatter model, and is well suited for the sparsely vegetated landscapes of the study site. In general, IEM quantifies the magnitude of backscattering as a function of moisture content and surface roughness, which are unknown, and the known radar configurations. Estimating surface roughness or soil moisture by solving the IEM with two unknowns is the core of the problems associated with the use of radar imagery coupled with IEM-like models. The conceptual model for solving this problem and mapping surface roughness and soil moisture without the use of ancillary data is outlined in Eq. (1) thru Eq. (6). To implement this model, the specific forms of Eqs. (2), (3) and (6) need to be derived in simple form for the radar image configurations used in this study. Because of the complex form of the IEM, analytically deriving these equations can be difficult. However, approximations of these equations with high level of precision may be possible by fitting polynomials with the IEM simulated data. This process is independent of field data and simply transforms IEM approximately into simple polynomials with parameter estimates.

With multiple runs of IEM, two data sets of σ^0 were simulated for the radar configurations similar to the June 9 and June 15 Envisat ASAR images (Table 1), and for valid combinations of L_c and h_{RMS} (Fig. 1). The moisture content θ_S was kept fixed at 0.03 m^3 m^{-3} to simulate a dry condition similar to the June 9 and June 15 images. The only difference in configuration between these two images, and therefore the two data sets, is the incidence angle (25° and 41°, respectively). The two data sets of backscatter were subtracted from one another ($\Delta\sigma^0$) and the z-index was computed from corresponding values of L_c and h_{RMS}. Backscatter difference was regressed with the z-index to get a best fit function to relate the two parameters, the general form of which is specified in Eq. (2). In order to get the specific form of Eq. (3), simulated backscatter associated with the June 15 image configuration was regressed with roughness parameters to fit a polynomial function of required order. The resulting equation, therefore, became an approximation of IEM under low moisture conditions, which is similar to the dry season. This procedure for determining the specific form of Eq. (3) was described in great detail by Rahman et al. (2007).

Two more data sets of IEM simulated backscatter were created for radar configurations similar to wet season images acquired on July 14 and August 2, 2004 (Table 1) and for valid combinations of L_c and h_{RMS} (Fig. 1) and θ_S (0.03 to 0.40 m^3 m^{-3}). For each data set the moisture content (θ_S) was regressed with simulated backscatter, L_c and h_{RMS} to fit a polynomial. These fitted polynomials represent the inverted IEM, which is specified in general terms in Eq. (6) for conditions on July 14 and August 2, 2004.

3. Results and discussion

The objectives of the study were to produce surface soil moisture and roughness maps using radar remote sensing data and to compare the map values with the ground measurements. The derivations of the specifics of the conceptual model to achieve the objectives are presented and their application for producing desired outputs are demonstrated. The strength and weaknesses of the whole approach are discussed.

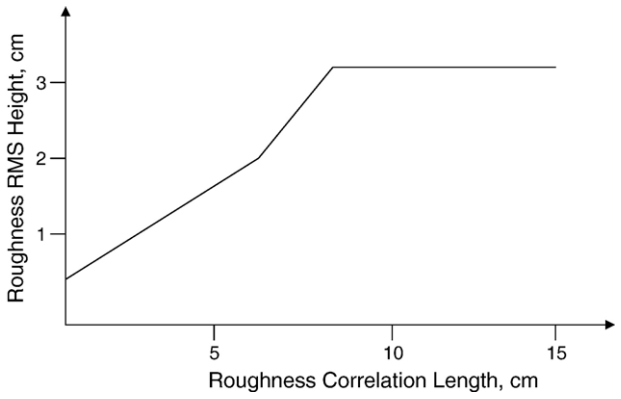

Fig. 1. The ranges of roughness parameters, correlation length (L_c) and RMS height (h_{RMS}), valid for IEM (area under the curve), Mametsa et al. (2002).

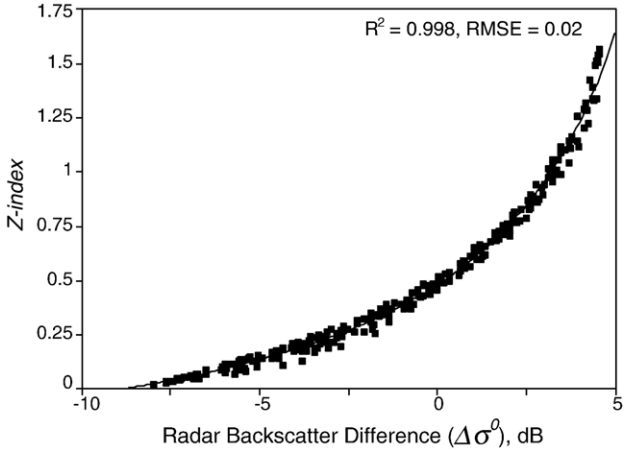

Fig. 2. Relation between roughness z-index ($h_{\mathrm{RMS}}^{2.5}/L_{\mathrm{c}}$) and radar backscatter difference ($\Delta\sigma^0$) between two images of same target under unchanged ground conditions with different incidence angle (41° and 25°) as specified in Eq. (7).

3.1. Mapping roughness

Surface roughness is often expressed by its statistical characteristic parameters, such as h_{RMS}, L_{c} and the shape of the autocorrelation function. In this study, mapping of surface roughness refers to mapping of h_{RMS} and L_{c}, while an a-priori assumption was made on the shape of the autocorrelation function. Mapping of h_{RMS} and L_{c} was achieved by explicitly solving the specific form of Eqs. (2) and (3) as indicated in Eq. (4) and described below.

The specific form of Eq. (2) was derived by the use of a simulated data set, the description of which is given before in the Radar Model and Implementation subsection. The data set included IEM-simulated backscatter difference ($\Delta\sigma^0$) between two incidence angles (25° and 41°), and the surface roughness and moisture information for which the data set was simulated. The incidence angles selected for simulation match the radar images acquired for roughness mapping (Table 1). Using that data set, a function was fitted through z-index and $\Delta\sigma^0$ to get a specific form of Eq. (2). It was found that the definitions of z-index as well as the specific functional form used by Zribi and Dechambre (2002) needed a slight change to better fit the radar configurations used in this study. With the newly defined z-index, which is $h_{\mathrm{RMS}}^{2.5}/L_{\mathrm{c}}$, the specific form of Eq. (2) became

$$h_{\mathrm{RMS}}^{2.5}/L_{\mathrm{c}} = (0.618 + 0.09\Delta\sigma^0)/(1 - 0.138\Delta\sigma^0), \tag{9}$$

with $R^2 = 0.998$ and RMSE = 0.02 (Fig. 2). Note that this is not an empirical model derived from field data, but rather, an approximation of IEM using simple functions based on IEM simulated data.

Plugging the backscatter difference ($\Delta\sigma^0$) between consecutive pixels of two images acquired over the study site with different incidence angles (25° and 41°) into the above equation, a map of z-index was produced. These images were acquired in the summer time under dry surface conditions over a short temporal interval (June 9 and June 15), thereby satisfying the invariant soil moisture, roughness and vegetation conditions on which Eq. (9) is based.

Derivation of Eq. (3) was achieved by the use of the IEM-simulated data set for dry surface condition and a single incidence angle (41°). The dry surface condition was simulated by the use of low and invariant value of moisture level ($\theta_{\mathrm{S}} = 0.03$ m^3 m^{-3}). The data set was described in the Radar Model and Implementation subsection. Following Rahman et al. (2007), a polynomial of required degree was fitted with the data to get the specific form of Eq. (3) as

$$\begin{aligned}\sigma_{\mathrm{dry}}^0 = {} & -27.94 + 32.58h_{\mathrm{RMS}} - 1.40L_{\mathrm{c}} - 18.78h_{\mathrm{RMS}}^2 \\ & + 0.05L_{\mathrm{c}}^2 + 0.86h_{\mathrm{RMS}}L_{\mathrm{c}} + 2.65h_{\mathrm{RMS}}^3 \\ & + 0.12h_{\mathrm{RMS}}^2L_{\mathrm{c}} - .04h_{\mathrm{RMS}}L_{\mathrm{c}}^2,\end{aligned} \tag{10}$$

where $R^2 = 0.987$ and RMSE = 0.65 (Fig. 3). Again, this is an approximation of IEM with a simple function. Multiple

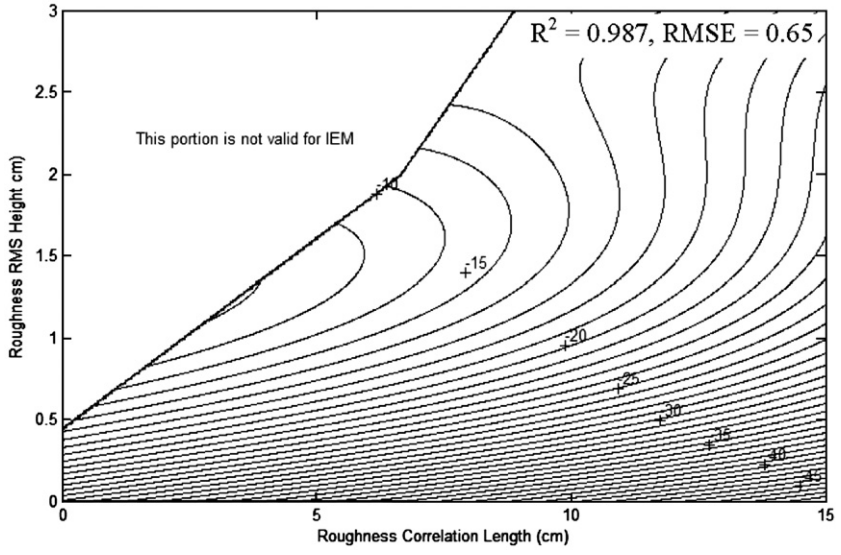

Fig. 3. IEM embedded relationship among roughness RMS height (h_{RMS}), correlation length (L_{c}) and Radar backscatter (σ^0) for a fixed moisture content, $\theta_{\mathrm{S}} = 0.03$ m^3 m^{-3}. The graphs are plots of Eq. (10) that approximates IEM with negligible moisture condition. The numbers inside the graphs are σ^0 in dB unit.

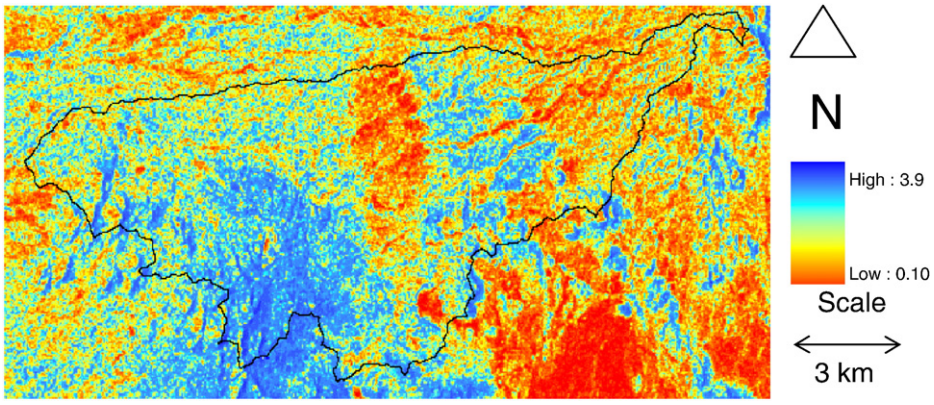

Fig. 4. Roughness map (h_{RMS} in cm) derived from radar images by the use of IEM, as formulated in Eq. (4). The solid line represents the boundary of USDA ARS Walnut Gulch Experimental Watershed.

solutions for h_{RMS} and L_c exist for a particular value of backscatter, which is an inherent character of IEM. The estimated equation reflects this character. The first solution is always accepted following Baghdadi et al. (2004).

The L_c as a function of h_{RMS} and z-index from Eq. (9) was substituted in Eq. (10) to obtain

$$\sigma^0_{dry} = -27.94 + 32.58h_{RMS} - 18.78h^2_{RMS} + 2.65h^3_{RMS} + \frac{1}{z-index}\left(-1.40{*}h^{2.5}_{RMS} + 0.86{*}h^{3.5}_{RMS} + 0.12{*}h^{4.5}_{RMS}\right) + \left(\frac{1}{z-index}\right)^2\left(0.05{*}h^5_{RMS} - .04{*}h^6_{RMS}\right). \quad (11)$$

This equation was solved numerically to obtain h_{RMS} as a function σ^0_{dry} and z-index (and z-index, in turn, as a function of $\Delta\sigma^0$). The resulting h_{RMS} was then substituted back in Eq. (9) to solve for L_c. Thus, the solution of h_{RMS} and L_c as a function of σ^0_{dry} and $\Delta\sigma^0$ indicated in Eq. (4) was achieved. Using Arc Info programming facilities, the solution process was conducted on a per-pixel basis, where the radar image acquired on June 15, 2004 was used for extracting σ^0_{dry} and the z-index map produced in an earlier stage was used for extracting the value of z-index of the corresponding pixel. The resulting value of h_{RMS} was assigned to the corresponding pixel of a new map referred to as h_{RMS} map (Fig. 4). The map of L_c was obtained by the simple Arc Info grid operation as $L_c = h^{2.5}_{RMS}/z$-index (Fig. 5). In Figs. 4 and 5, blue colors represent high roughness, which seem to be associated with the mountainous areas, for both h_{RMS} and L_c. The river stream beds and adjacent areas, and mountain valley areas look smoother with low roughness values represented by the red color. In this application, Eq. (10) was derived for a fixed incidence angle, close to angles of the experimental fields. Error might increase with distance from these fields and with changes in local incidence angle caused by rough terrain.

3.2. Mapping soil moisture

The general framework for estimating soil moisture through parameterizing IEM with the image-derived roughness maps was provided in Eq. (6). In order for the framework to be operational, the approximate specific form of Eq. (6) needed to be determined. IEM simulated data were used again for this purpose. This time the radar configurations were chosen to simulate July 14 and August 2, 2004 images for valid combinations of h_{RMS}, L_c and θ_S. Using the data set in a regression analysis, Eq. (12) and Eq. (13) were derived as approximations of Eq. (6) for July 14 and August 2, 2004 respectively. These are fourth order polynomial equations, for which multiple solutions are theoretically possible. However, within the domain of our parameter values unique

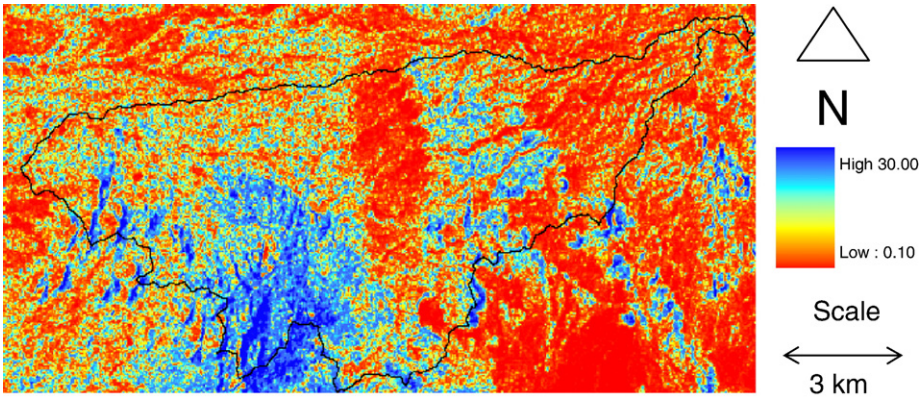

Fig. 5. Roughness map (L_c in cm) derived from radar images by the use of IEM, as formulated in Eq. (4). The solid line represents; the boundary of USDA ARS Walnut Gulch Experimental Watershed.

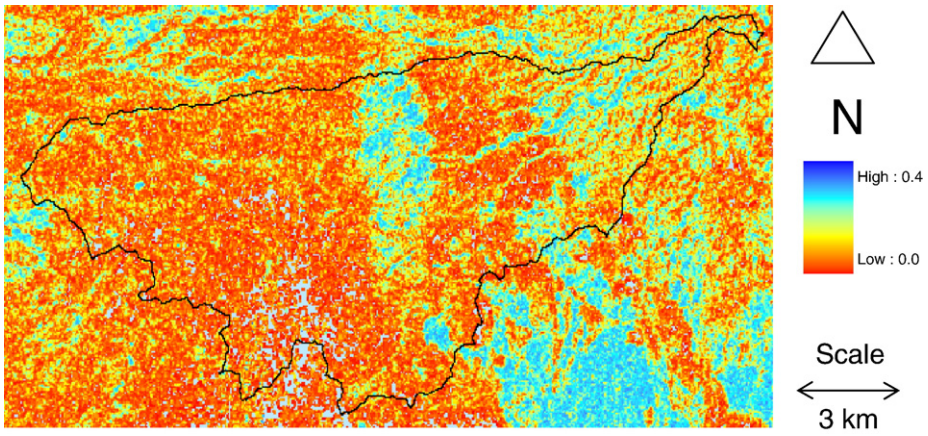

Fig. 6. Soil moisture map (in $m^3\ m^{-3}$) for July 14, 2004 derived from radar images by the use of IEM, as formulated in Eq. (6). The solid line represents the boundary of USDA ARS Walnut Gulch Experimental Watershed. A similar soil moisture map was produced for August 2, 2004, but the maps were nearly identical in color and the second map was not included here.

solutions for soil moisture were achieved. As with Eqs. (9) and (10), Eqs. (12) and (13) were not derived from field data, but from an approximation of the inverted IEM.

$$\begin{aligned}\ln(\theta_S) = {} & .353 + 1.384\ln(-\sigma^0) - .913\{\ln(-\sigma^0)\}^2 \\ & -1.735\ln(L_c) + .947\{\ln(L_c)\}^2 + .013\{\ln(L_c)\}^3 - .017\{\ln(L_c)\}^4 \\ & -1.791\ln(h_{RMS}) + 5.475\{\ln(h_{RMS})\}^2 + .743\{\ln(h_{RMS})\}^3 \\ & +.087\{\ln(h_{RMS})\}^4 - 1.95\ln(h_{RMS})\ln(L_c) \\ & -1.0\{\ln(h_{RMS})\}^2\ln(L_c) - .187\{\ln(h_{RMS})\}^3\ln(L_c) \\ & +.006\{\ln(L_c)\}^2\ln(h_{RMS}) + .048\{\ln(L_c)\}^3\ln(h_{RMS}) \\ & +.055\{\ln(L_c)\}^2\{\ln(h_{RMS})\}^2 + 1.291\ln(-\sigma^0)\ln(h_{RMS}) \\ & +.1\ln(-\sigma^0)\ln(L_c) - .112\ln(-\sigma^0)\{\ln(L_c)\}^2 \\ & -.79\ln(-\sigma^0)\{\ln(h_{RMS})\}^2\end{aligned} \tag{12}$$

where $R^2 = 0.996$ and RMSE = 0.04.

$$\begin{aligned}\ln(\theta_S) = {} & -.064 + 1.765\ln(-\sigma^0) - .986\{\ln(-\sigma^0)\}^2 \\ & -1.83\ln(L_c) + .866\{\ln(L_c)\}^2 + .028\{\ln(L_c)\}^3 - .019\{\ln(L_c)\}^4 \\ & -.515\ln(h_{RMS}) + 5.366\{\ln(h_{RMS})\}^2 + .885\{\ln(h_{RMS})\}^3 \\ & +.112\{\ln(h_{RMS})\}^4 - 2.089\ln(h_{RMS})\ln(L_c) \\ & -1.071\{\ln(h_{RMS})\}^2\ln(L_c) - .197\{\ln(h_{RMS})\}^3\ln(L_c) \\ & +.017\{\ln(L_c)\}^2\ln(h_{RMS}) + .048\{\ln(L_c)\}^3\ln(h_{RMS}) \\ & +.053\{\ln(L_c)\}^2\{\ln(h_{RMS})\}^2 + 1.003\ln(-\sigma^0)\ln(h_{RMS}) \\ & +.07\ln(-\sigma^0)\ln(L_c) - .084\ln(-\sigma^0)\{\ln(L_c)\}^2 \\ & -.688\ln(-\sigma^0)\{\ln(h_{RMS})\}^2\end{aligned} \tag{13}$$

where $R^2 = 0.996$ and RMSE = 0.04.

The inversion of IEM derived in Eqs. (12) and (13) was implemented in the Arc Info grid environment to produce soil moisture (θ_S) maps, where image-derived roughness maps (h_{RMS} and L_c) and radar images (σ^0) under wet condition were used as inputs. Thus, soil moisture maps were produced for the images acquired on July 14 and August 2, 2004 (Fig. 6). In Fig. 6, the dominant red colors in the map represent low level of moisture across almost the entire watershed, except river streams and mountain valley areas, where the color is bluish representing relatively higher level of moisture. However, this map may contain some error caused by varying incidence angles in locations far from the experimental fields and in rough terrain.

3.3. Field validation of surface roughness and soil moisture maps

Field measurements of soil moisture were made over the 110 by 110 m area of each of the 13 sample sites, whereas measurements of roughness are made over a 35 by 35 m area. The 110 by 110 m areas corresponding to each sample site were identified on the soil moisture maps based on their known coordinates for clipping. The same operation was conducted on the surface roughness map, but the clipped areas were 35 by 35 m. The average of the map values within clipped areas was compared with the field measured values of roughness (Figs. 7 and 8) and soil moisture (Fig. 9).

It was found that the field-data-derived surface roughness parameters were generally low both for h_{RMS} and L_c compared to the same derived from radar images (Table 3). The image-derived h_{RMS} and L_c averaged over all experiment locations were 2.19 cm and 13.3 cm as opposed to 0.79 cm and 8.2 cm respectively for field measurements. This may be a confirmation

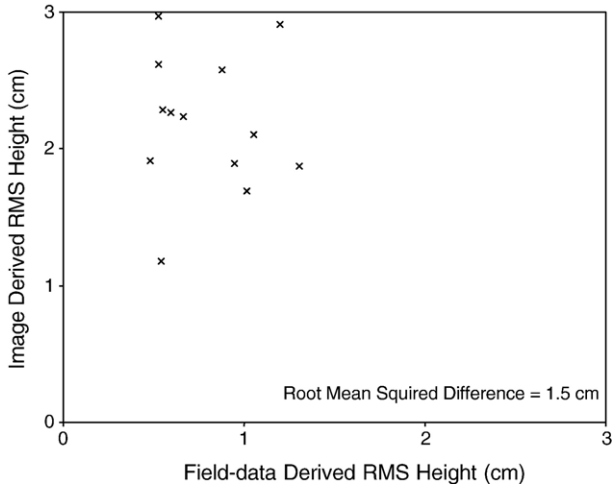

Fig. 7. Comparison of roughness (h_{RMS}), where field measurements from 13 experimental sites were plotted in the x-axis and image-derived roughness estimates extracted from same sites were plotted in the y-axis.

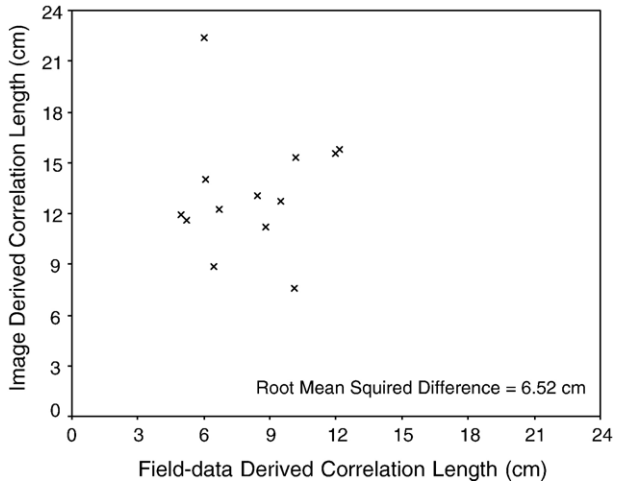

Fig. 8. Comparison of roughness (L_c), where field measurements from 13 experimental sites were plotted in the x-axis and image-derived roughness estimates extracted from same sites were plotted in the y-axis.

that the subsurface roughness caused by the rock fragments plays an important role. The radar signal is probably responsive to multiple bounce by the subsurface rock fragments when it penetrates a few centimeters below ground surface. As a result, radar-perceived roughness may be much larger than that of field measurements. The roughness-measuring field device was not designed to account for subsurface nature of roughness. Therefore, roughness measurements by the pin meter may not be adequate to characterize surface roughness for input to IEM, especially for study sites with large amounts of rock fragments.

Concerning soil moisture, good association between image-derived soil moisture and averaged field measured soil moisture were found once the field measured soil moisture was adjusted for the effects of rock fragments (Fig. 9, Table 4). The image-derived moisture contents averaged over all experiment locations are

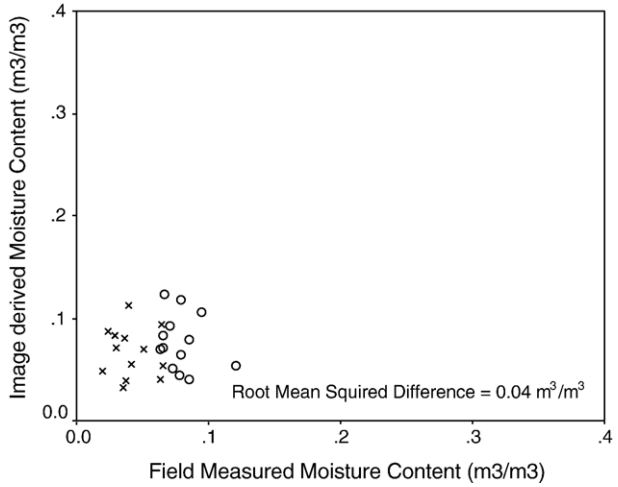

Fig. 9. Validation soil moisture maps, where field measurements from 13 experimental sites were plotted in the x-axis and, image-derived moisture estimates extracted from same sites were plotted in the y-axis. Cross signs are points associated with July 14, 2004 overpass of Envisat and the circles are with August 2, 2004.

Table 3
Comparisons of roughness measurements by image data

Validation	Mean	SD	Min	Max
L_c derived from field measurements by pin meter, cm	8.20	2.42	4.98	12.15
L_c derived from image data, cm	13.25	3.60	7.61	22.43
h_{RMS} derived from field measurements by pin meter, cm	0.79	0.28	0.48	1.30
h_{RMS} derived from image data, cm	2.19	0.49	1.17	2.97

0.07 m^3 m^{-3} and 0.08 m^3 m^{-3} for July and August as opposed to 0.04 m^3 m^{-3} and 0.07 m^3 m^{-3} respectively for field measured moisture content. Thoma et al. (2006) presented similar evidence for the same watershed following a different technique. It appears that radar remote sensing is successful in providing good estimates of soil moisture at a watershed scale, although its success at the field scale remains uncertain.

In this study there are a number of potential sources of errors that may have some association with the uncertainty in the result at the field scale, which is evident in the scattering of points in the Fig. 9. The adjustment of field measured soil moisture concerning rock fragments involves reducing the field measured moisture content by the average proportion of rock fragment in the study site, which is 47%, to represent moisture content of rock–soil composite. This computation was based on the assumption that the rock contains negligible amounts of moisture and the Theta Probe measured moisture constitutes the soil portion of the rock–soil composite. It was further assumed that all experiment locations had the same rock fragment content, the magnitude of which was equal to the watershed average. This later assumption may have some impact on the accuracy of the results, given the unavailability of rock fragment data for all study locations.

Another source of error in the field validation may be related to the method of speckle reduction. A median filter consisting of a 9-pixel moving window was applied for speckle reduction, which may not be adequate. Theoretically, speckle is random error added to the pixel values of an image, which is inherent to the radar remote sensing. The terrain of the watershed under

Table 4
Watershed scale field validation of soil moisture measurements by image data

Validation	Mean	SD	Min	Max
July 14, 2004				
θ_S by field measurements, m^3 m^{-3}	0.04	0.01	0.02	0.06
θ_S derived by image data, m^3 m^{-3}	0.07	0.02	0.03	0.11
θ_S derived by IEM using field measured roughness, m^3 m^{-3}	0.16	0.10	0.03	0.35
August 2, 2004				
θ_S by field measurements, m^3 m^{-3}	0.07	0.01	0.05	0.10
θ_S derived by image data, m^3 m^{-3}	0.08	0.03	0.04	0.12
θ_S derived by IEM using field measured roughness, m^3 m^{-3}	0.15	0.10	0.04	0.35
Over all				
θ_S by field measurements, m^3 m^{-3}	0.05	0.02	0.02	0.10
θ_S derived by image data, m^3 m^{-3}	0.07	0.03	0.03	0.12
θ_S derived by IEM using field measured roughness, m^3 m^{-3}	0.15	0.09	0.03	0.35

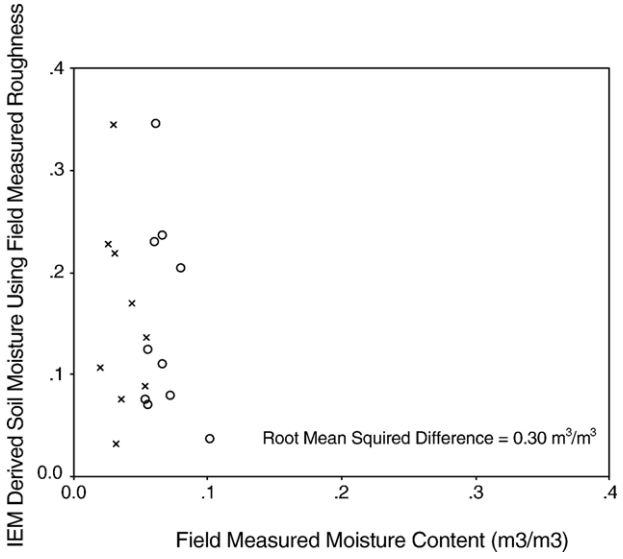

Fig. 10. Performance of radar backscatter model, when field measurements of roughness are used as inputs. Cross signs are points associated with 13 experimental sites on July 14, 2004 overpass and the circles are with August 2, 2004. In few cases IEM predicted moisture content fall outside valid range; these points are not included in the graph.

study, which is rolling mountain, may seem a source of potential error, since a terrain correction was not applied. However, the sites chosen for the study were flat and should not be a major concern. The way equations were derived to form the framework of an equation-based solution may also have some impact on the results. A fixed incidence angle was chosen for deriving each equation. This may appear problematic since the equations were applied in pixel-by-pixel computation for the entire image for which the incidence angles varied block wise. However, since the experiment locations were closely spaced, the difference in incidence angles among locations were very small and the assumption of fixed incidence angle may not be a big problem after all.

The results presented in Fig. 9 using image-derived estimates of roughness can be compared to the performance of IEM when the field measurements of roughness were used as inputs to the model (Fig. 10 and Table 4). It was found that the image-derived roughness perform far better in parameterizing IEM for soil moisture retrieval. This finding may be evidence that it is probably the input parameters that result in poor performance of the IEM model rather than the model itself. This may also be considered an indirect and aggregated precision of the image-derived roughness parameters estimated in this study.

4. Conclusions

In previous studies, radar images have been used for retrieving distributed surface soil moisture based on field measurements of surface roughness data used to parameterize the IEM. The estimation of the characteristic parameters of surface roughness using field data has been unreliable and the measurement of roughness itself is cumbersome and infeasible for large scale application. In this study, a method was developed to map characteristic parameters of surface roughness using radar images as a replacement for field-collected ancillary data. The method-driven estimates of soil moisture were validated against field measurements. Results indicate that there is good association between image-derived soil moisture and field measured soil moisture. Moreover, the implementation of this method is rather straight forward (Fig. 11). It involves approximation of IEM and some of its derivatives with simple functions using model simulated data and the manipulations of these functions by the use of image data and ArcInfo programming.

It was found that the image-derived surface roughness was larger than field measured roughness. This may confirm that the subsurface roughness caused by the rock fragments plays an important role. Radar signal is probably responsive to multiple bounce by the subsurface rock fragments when it penetrates few centimeters below ground surface, in addition to the scattering due to surface roughness. As a result, radar-perceived roughness may be much larger than that of field measurements. The roughness measuring field device is not designed to account for subsurface roughness. Therefore, roughness measurements by the pin meter may not be adequate to characterize surface roughness for inputting in IEM, especially for study sites with large amounts of rock fragments.

The conditions, under which the model is developed, applied and validated, are best suited to its application in rangelands, where the vegetation is sparse, precipitation is low and the surface roughness does not change between dry and wet periods. To broaden the applicability of the model to agricultural land, especially in the mature stage of crop growth when the vegetation becomes dense, additional validation work must be conducted. In particular, future research must investigate the application of the model under a broader range of vegetation and moisture conditions. If the model is not applicable in areas of dense vegetation (agricultural land for example), additional research should be conducted to incorporate a variable reflecting vegetation cover or density into the model. Further, the method developed in this study is applied for C-band radar image and its applicability for other radar frequencies needs to be determined.

The model developed through this research required the use of dry season radar images for estimation of surface roughness. Agricultural land preparation may change surface roughness between dry and wet periods. As a result surface roughness estimated from dry images may not be applicable to a wet image for soil moisture estimation. Future research is therefore needed to either establish the error introduced or eliminate the requirement for a dry season images for roughness estimation.

The method developed in this study also depends on the use of radar images from two different view angles, which can be acquired from existing radar sensors given a time span of the repeat cycle of the satellite. However, the moisture or roughness conditions may undergo change within this time-frame making the method developed here less applicable. The capability of a radar sensor to acquire data at multiple view angles at the same time should be considered in the design of future radar systems. In addition, future research into the feasibility of replacing the need for images at two-view angles with images at two different polarizations could be beneficial. Existing radar sensors already

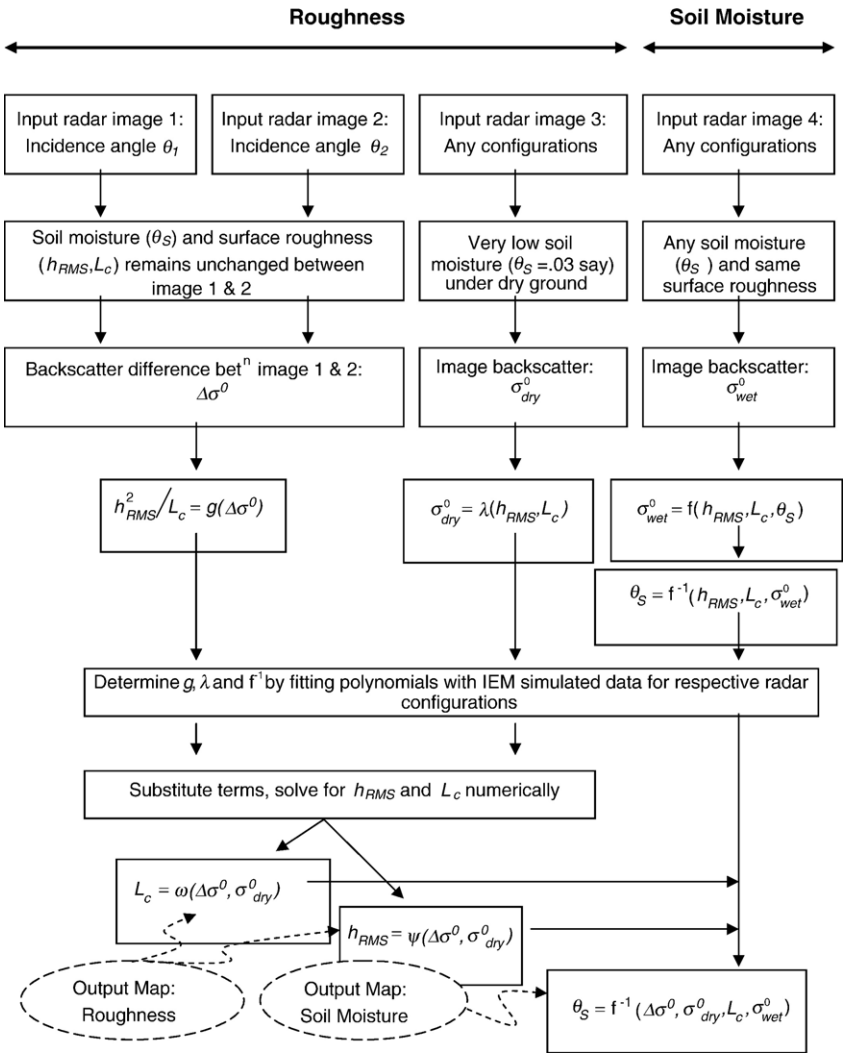

Fig. 11. Schematic diagram of the steps followed for the image-based mapping of surface soil moisture and roughness. Note that if image 1 and 2 are acquired in dry condition, one of them can serve as image 3.

have the capability of simultaneously acquiring images at multiple polarizations. This would eliminate errors introduced due to registration inaccuracy when merging the images at two-view angles. Research in any one of these directions is highly recommended.

Acknowledgements

All authors appreciate the support of the US Army Engineer Research and Development Center, Topographic Engineering Center. We would like to thank all the people that made our field work possible at the USDA ARS Walnut Gulch Experimental Watershed.

References

Baghdadi, N., Gherboudj, I., Zirbi, M., Sahebi, M., King, C., & Bonn, F. (2004). Semi-empirical calibration of the IEM backscattering model using radar images and moisture and roughness field measurements. *International Journal of Remote Sensing*, *25*(18), 3593−3623.

Baghdadi, N., Paillou, P., Grandjean, G., Dubois, P., & Davidson, M. (2000). Relationship between profile length and roughness variables for natural surfaces. *International Journal of Remote Sensing*, *21*(17), 3375−3381.

Bryant, R., Moran, M. S., Thoma, D. P., Holifield, C. D., Skirvin, S., Rahman, M. M., et al. (2007). Measuring surface roughness to parameterize radar backscatter models for retrieval of surface soil moisture. *Geoscience and Remote Sensing Letters*, *4*(1).

Davidson, M. W. J., Le Toan, T., Mattia, F., Satalino, G., Manninen, T., & Borgeaud, M. (2000). On the characterization of agricultural soil roughness for radar remote sensing studies. *IEEE Transactions on Geoscience and Remote Sensing*, *38*(2), 630−640.

ESA (2002, December). *European space agency–Envisat ASAR Product Handbook, Issue 1.1.*

Fung, A. K. (1994). *Microwave scattering and emission models and their applications.* Norwood, MA: Artech House.

Fung, A. K., Li, Z., & Chen, K. S. (1992). Backscattering from a randomly rough dielectric surface. *IEEE Transactions on Geoscience and Remote Sensing*, *30*(2), 356−369.

Fung, A. K., & Pan, G. W. (1986). An integral equation model for rough surface scattering. *Proceedings of the International Symposium on Multiple Scattering of Waves in Random Media and Random Rough Surface, 29 July–2 August 1985, University Park, PA* (pp. 701−714). Pennsylvania State University Press.

Jackson, T. J., Kostov, K. G., & Saatchi, S. S. (1992). Rock fraction effects on the interpretation of microwave emission from soil. *IEEE Transactions on Geoscience and Remote Sensing*, *30*(3), 610−616.

Le Toan, T., Davidson, M., Mattia, F., Borderies, P., Chenerie, I., Manninen, T., et al. (1999). Improved observation and modelling of bare soil surfaces for soil moisture retrieval. Special issue: Retrieval of bio-and geo-physical parameters from SAR data for land applications. Papers from the 2nd International Workshop, Noordwijk, Netherlands, 21–23 October 1998. *Earth-Observation-Quarterly.* 1999, No. 62, 20–24; 6 ref. European Space Agency; Noordwijk; Netherlands.

Mametsa, H. J., Koudogbo, F., & Combes, P. F. (2002). Application of IEM and radiative transfer formulations for bistatic scattering of rough surfaces. *IEEE Transactions on Geoscience and Remote Sensing*, *1*, 24−28.

Moran, M. S., Peters-Lidard, C. D., Watts, J. M., & McElroy, S. (2004). Estimating soil moisture at the watershed scale with satellite-based radar and land surface models. *Canadian Journal of Remote Sensing*, *30*, 1−22.

Rahman, M. M., Moran, M. S., Thoma, D. P., Bryant, R., Sano, E. E., Holifield–Collins, C. D., et al. (2007). "A derivation of roughness correlation length for parameterizing radar backscatter models". *International Journal of Remote Sensing*, *28*(18), 3995−4012.

Renard, K. G., Lane, L. J., Simanton, J. R., Emmerich, W. E., Stone, J. J., Weltz, M. A., et al. (1993). Agricultural impacts in an arid environment: Walnut Gulch studies.*American Institute of Hydrology, Hydrological Science and Technology*, *9*(1–4), 145−190 (SWRC Reference No.: 921).

Staples, G., & Branson, W. (1998). *Radarsat illuminated, your guide to products and services. Radarsat International, 13800 Commerce Pkwy, MacDonald Dettwiler Bldg. Richmond B.C., Canada V6V 2J3.*

Thoma, D., Moran, M. S., Bryant, R., Rahman, M. M, Holifield, C., & Skirvin, S. (2006). Comparison of two methods for extracting surface soil moisture from C-band radar imagery. *Water Resources Research*, *42*, W01418. doi:10.1029/2004WR003905

U.S. Department of Agriculture (2002). Soil Survey of Cochise County, Arizona, Douglas-Tombstone Part, Nat. Resour. Conserv. Serv., Washington, D.C.

Verhoest, N. E. C., Hoeben, R., De Troch, F. P., & Troch, P. A. (2000). Soil moisture inversion from ERS and SIR-C imagery at the Zwalm catchment, Belgium. *Geoscience and Remote Sensing Symposium, 2000. Proceedings. IGARSS. IEEE 2000 International*, *Vol. 5, 24–28*. (pp. 2041−2043).

Zribi, M., & Dechambre, M. (2002). A new empirical model to retrieve soil moisture and roughness from C-band radar data. *Remote Sensing of Environment*, *84*, 42−52.